Brazilian Journal
of Chemical
Engineering

ISSN 0104-6632
Printed in Brazil
www.abeq.org.br/bjche

Vol. 36, No. 01, pp. 265 - 273, January - March, 2019
dx.doi.org/10.1590/0104-6632.20190361s20180067

NI-MO SUPPORTED NANOPOROUS GRAPHENE AS A NOVEL CATALYST FOR HDS AND HDN OF HEAVY NAPHTHA

Babak Behnejad[1], Majid Abdouss[1*] and Ahmad Tavasoli[2]

[1] Amirkabir University of Technology, Department of Chemistry, Tehran, Iran.
E-mail: phdabdouss44@aut.ac.ir, ORCID: 0000-0003-2305-7985
[2] University of Tehran, College of Science, School of Chemistry, Tehran, Iran.

(Submitted: February 17, 2018 ; Revised: April 13, 2018 ; Accepted: April 24, 2018)

Abstract - Reducing sulfur and nitrogen compounds is essential in producing clean fuels for providing a green environment. In this regard, a novel nanocatalyst has been proposed for Hydrodesulfurization (HDS) and Hydrodenitrogenation (HDN) of heavy naphtha. To this end, Ni-Mo was loaded on nanoporous graphene (Ni-Mo/NG) through the incipient wetness impregnation method. The synthesized nanocatalyst was characterized by FE-SEM, ICP, BET, FTIR, XRD and TPR methods. The catalytic activity of the Ni-Mo/NG catalyst was evaluated at 290°C and 30 bar. For the synthesized Ni-Mo/NG catalyst, conversions of total sulfur, total nitrogen and R-SH compounds (mercaptans) were obtained as 99.5, 99.4 and 99.3%, respectively, which shows considerable enhancement in comparison to the Ni-Mo/γ-Alumina industrial catalyst.
Keywords: HDS; HDN; Nanocatalyst; Ni-Mo/nanoporous graphene; Naphtha.

INTRODUCTION

Treating and reducing sulfur and nitrogen compounds is still a challenging issue which must be addressed. The presence of these compounds in fuels contributes to environmental pollution, which must be reduced. Therefore, the amount of sulfur and nitrogen compounds in fuels should be decreased to provide a clean environment. Hydrodesulfurization (HDS) (Gao et al., 2011; González-Cortés et al., 2006; Hajjar et al., 2015, 2016a, 2017a, 2017b; Huirache-Acuña et al., 2012; Mendoza-Nieto et al., 2015; Miller et al., 2000; Shan et al., 2015) and hydrodenitrogenation (HDN) (Sundaramurthy et al., 2006; Zepeda et al., 2016) are the main processes considered for reducing the Total Sulfur (T.S.) and Total Nitrogen (T.N.) of various fractions.

Molybdenum-based catalysts activated by nickel or cobalt have been widely studied for HDS of various fractions. Vonortas and Papayannakos (2014) studied the effect of free fatty acids on the HDS activity of Co-Mo/γ-Al_2O_3 on atmospheric heavy gas oil. An ordered mesoporous NiMo-Al_2O_3 catalyst was prepared by Liu et al. (2016) for HDS of dibenzothiophene and they reported the Ni/Mo molar ratio of 1:1 for high HDS activity. Klimov et al. (2016) prepared a CoNiMo/Al_2O_3 catalyst for deep HDT of vacuum gas oil and found that the catalyst with 1.8% Co, 1.2% Ni and 10% Mo has the highest activity in hydrotreating of vacuum gas oil. Mendoza-Nieto et al. (2015) studied the effect of support on the catalytic performance of NiMoW in HDS of dibenzothiophenes; they used SBA-15 silica and conventional gamma-alumina as catalyst support and reported that the best dispersion of Mo and W species was obtained on SBA-15, which showed the highest HDT performance.

Also in various recent works, carbon-based materials have been used as catalyst support. Dong et al. have used multi-walled CNTs as support for a Co-Mo sulfide catalyst in HDS of thiophene and HDN of

* Corresponding authors: Majid Abdouss - E-mail: phdabdouss44@aut.ac.ir

pyrrole, which could considerably increase the HDT reactions (Dong et al., 2006). Furthermore, carbon nanofiber as catalyst support of Co/Ni/Mo catalysts (Yu et al., 2008) and multi-walled CNT as catalyst support of NiMo (Eswaramoorthi et al., 2008) and CoMo (Khorami and Kalbasi, 2011) were considered for HDT processes. Soghrati et al. (2012) supported the Co-Mo catalyst on CNT coated cordierite monoliths for HDS of naphtha, which showed better results compared with that of the CoMo catalyst. Moreover, activated carbon has also been used as catalyst support of NiMo in HDT of light gas oil (Rambabu et al., 2014). Recently, graphene has been widely used as an efficient catalyst support (Al-Daous, 2015; Hajjar et al., 2016a, 2016b, 2017a; Julkapli and Bagheri, 2015; Liu et al., 2014; Wang et al., 2015). Liu et al. (2014) prepared MoS_2/graphene nanocomposites for HDS of carbonyl sulfide; Wang et al. (2015) supported the NiMo over graphene-modified mesoporous TiO_2 for HDS of dibenzothiophene, which reported desirable results for graphene as an efficient catalyst support. Also, a graphene-MoS_2 composite was used by Al-Daous (2015) for HDS of dibenzothiophene, who reported that higher HDT activity is obtained for the composites with larger MoS_2 particles. Finally, Hajjar et al. (2017) used a Co-Mo/graphene catalyst through spray pyrolysis for HDS of naphtha (Hajjar, Kazemeini, Rashidi, Soltanali, et al., 2017), which showed a conversion of 100%.

Herein, we report the first use of Ni-Mo supported nanoporous graphene for HDS and HDN of heavy naphtha. As nanoporous graphene possesses high surface area and pore volume, it can distribute the Ni-Mo particles well. So, the active phases are well exposed to the reactant material. As the first report regarding the application of Ni-Mo supported nanoporous graphene, the prepared catalysts are thoroughly characterized and the performance of the prepared novel catalyst is evaluated. The catalytic activity of the synthesized novel nanocatalyst has been compared with that of the industrial Ni-Mo/γ-Alumina catalyst.

EXPERIMENTAL

Materials

Nanoporous graphene (NP) was purchased from RIPI (Research Institute of Petroleum Industry, National Iranian Oil Company), Iran. Sulfuric acid 98%, Nitric acid 30%, analytical grade nickel nitrate hexahydrate ($Ni(NO_3)_2 \cdot 6H_2O$), ammonium heptamolybdate tetrahydrate ($(NH_4)_6Mo_7O_{24} \cdot 4H_2O$) and dimethyldisulfide (DMDS) were supplied by Merck Chemical Co. In addition, analytical grade H_2 and deionized water (DI) were used throughout the experiments.

Treatment of catalyst support

Prior to preparation of the catalyst, NP particles were functionalized using H_2SO_4/HNO_3 acid with a ratio of 3:1. For this purpose, the vapor of this acid mixture was used for functionalizing the NG particles which is different from the preparation of graphene oxide. In this method, functional groups of carboxylic acid are added on the graphene surface.

Nanocatalyst preparation

For preparing the Ni-Mo/NG catalyst, the incipient wetness impregnation method was used. In this method, first molybdenum particles are loaded over nanoporous graphene. Ammonium heptamolybdate tetrahydrate was dissolved in DI water and this solution was added to the NP particles. Then the wet NP particles were heated to 120°C at a heating rate of 1°C/min and kept at that temperature for 4-h in an argon atmosphere. In the next step, the same procedure was utilized for loading nickel particles (by using nickel nitrate hexahydrate) on the the prepared Mo/NG sample. Then the calcination process was performed at 350°C for 4-h.The final Ni-Mo loaded nanoporous graphene is labeled as Ni-Mo/NG.

Nanocatalyst characterization methods

For characterizing the synthesized nanocatalyst, the X-ray diffraction (XRD) method was used for determining the crystalline phases formed (XRD PHILIPS PW1730, Netherland). Field Emission-Scanning Electron Microscopy (FE-SEM) was employed for investigating the morphology of the nanocatalyst by using the FESEM TESCAN MIRA, Czech device. The BET Belsorp Mini instrument was used for obtaining nitrogen adsorption/desorption isotherms, BET specific surface area, total pore volume, and pore size distribution. The Bruker device, made in Germany, was adopted for obtaining the FTIR spectra of the nanoporous graphene after functionalizing. Inductively coupled plasma-optical emission (ICP-OES) spectrometry was used for determining the metal loading which is an important factor in catalytic activity (Perkin Elmer, Optima 8000 Dual views). The temperature-programmed reduction (TPR) experiment was performed on the Ni-Mo/NG sample to obtain an H_2-TPR profile. For this purpose, the Micromeritics Chemisorb 2750 device was used.

Experimental outline and reaction testing

A continuous fixed-bed stainless steel reactor was used for performing the HDS and HDN reactions. The down-flow direction of the flow was used in the reactor. The schematic of the experimental catalyst evaluation setup is shown in Fig. 1.

In this setup, the reactor is 10 mm in inner diameter and 450 mm in length. The feedstock (liquid phase)

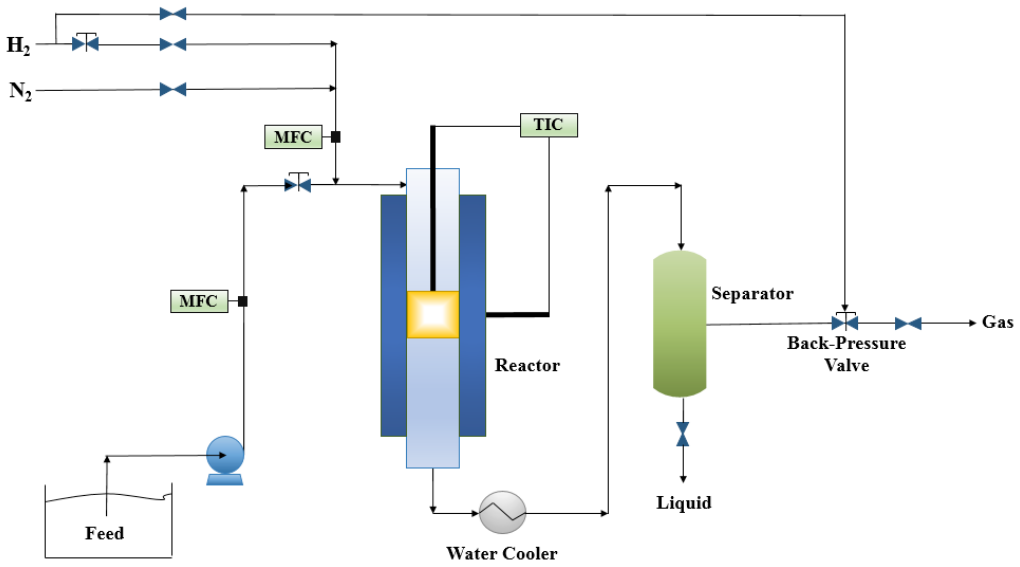

Figure 1. The simplified experimental reactor setup.

was inserted into the reactor and it was controlled by an HPLC pump (KNAUER K-501). The mass flow controller (Brooks 5850) device was employed for injecting hydrogen into the reaction section. The pressure of the reaction system was controlled by a backpressure valve and the reaction temperature was adjusted by an electrical heater. TIC WEST 3400 was adopted for monitoring and controlling the reaction temperature. In general, 1g of the synthesized nanocatalyst was loaded into a central segment of the reactor between two layers of carborundum filler and glass beads. After performing the leak test with nitrogen, the sweeping nitrogen gas was switched to hydrogen gas and the pressure was decreased until reaching the desired reaction pressure.

For providing the sulfide phase of Ni-Mo, all fresh catalysts were initially sulfided by using dimethyl disulfide (DMDS) and thereby the oxide phases were converted to an activated form (i.e. sulfide phase). The conventional industrial procedure was followed for performing the sulfiding process. The sulfiding process was done in two steps and the corresponding reaction conditions are shown in Table 1. At first, with a heating rate of 30°C/h, the temperature was increased up to 220°C in which DMDS was injected for 4 hours. Then, with a heating rate of 30°C/h, the temperature was increased to 330°C and DMDS was injected for another 12 hours.

Table 1. Sulfiding conditions prior to the HDS and HDN processes.

Sulfiding Conditions / Parameter	Sulfiding (1st Step)	Sulfiding (2nd Step)
Temperature, °C	220	330
Pressure, bar	35	35
LHSV, h^{-1}	3	3
H_2/HC, NL/L	115	115
Time, h	4	12

In the following, heavy naphtha was fed into the reactor and the catalytic reaction was started. The reaction temperature, pressure, LHSV, and H_2/HC ratio were adjusted for performing HDS and HDN reactions as shown in Table 2. The liquid sample was collected after reaching steady state conditions for which total sulfur, mercaptans and total nitrogen were determined.

Table 2. Reaction conditions in the HDS and HDN process in this research.

Sample / Parameter	Heavy naphtha
Temperature, °C	290
Pressure, bar	30
LHSV, h^{-1}	3.3
H_2/HC, NL/L	100

RESULTS AND DISCUSSION

Catalyst characterization tests

Due to the novelty of the synthesized nanocatalyst, quantitative and qualitative characterization methods were used for studying the Ni-Mo/NG sample. The FTIR spectrum was recorded from functionalized graphene prior to metal loading so that functional groups formed could be determined. In the FTIR spectrum of the sample, which is shown in Fig. 2, peaks at 3424, 2922, 2854, 1631, 1389, 1258, 1114, and 804 cm^{-1} are observed, which correspond to O-H, CH, CH, C=N, CH_2 or CH_3, C-O, C-O, and C-H bonds, respectively. Regarding the bonds that are formed after the functionalizing process, it can be deduced that carboxylic groups are introduced on the nanoporous graphene. It is reported that the presence of the peaks at about 3424 cm^{-1} confirms the presence of carboxylic functional groups on the sample (Fan et al., 2010; Huang et al., 2011).

Nitrogen adsorption/desorption of the Ni-Mo/NG catalyst (Fig. 3) exhibits the Type 4 isotherm, indicating that the synthesized nanocatalyst is mesoporous.

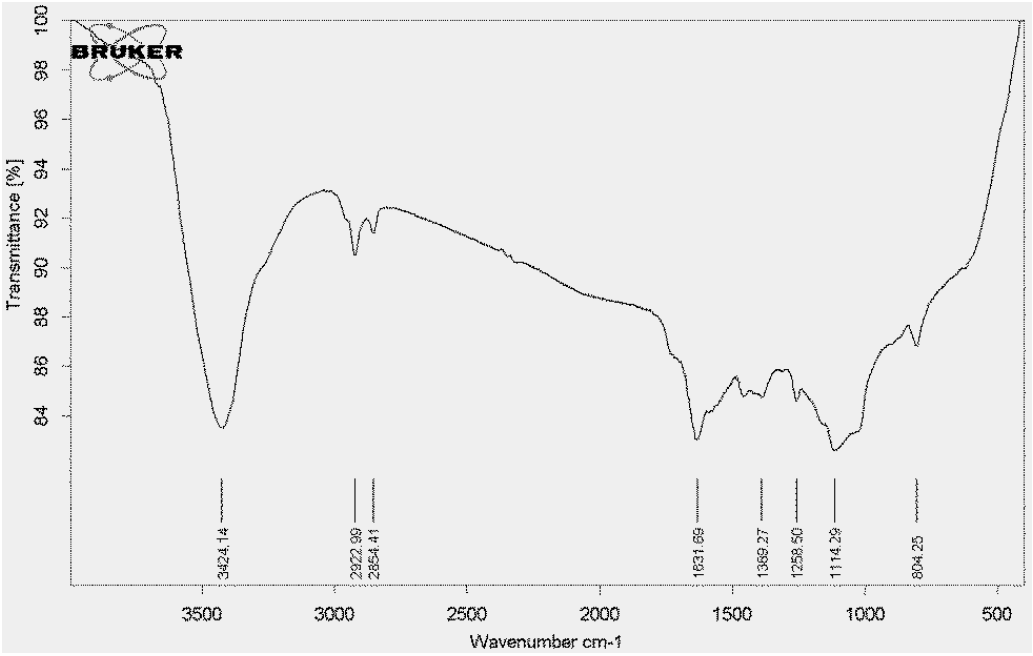

Figure 2. FTIR spectrum of the nanoporous graphene after functionalizing.

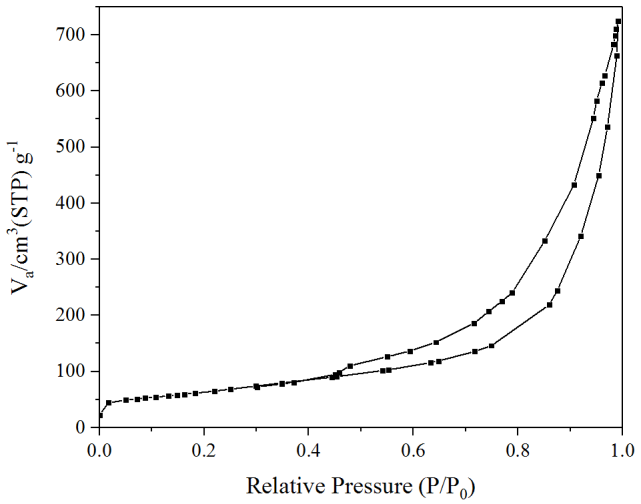

Figure 3. Nitrogen adsorption/desorption isotherm obtained for the Ni-Mo/NG catalyst.

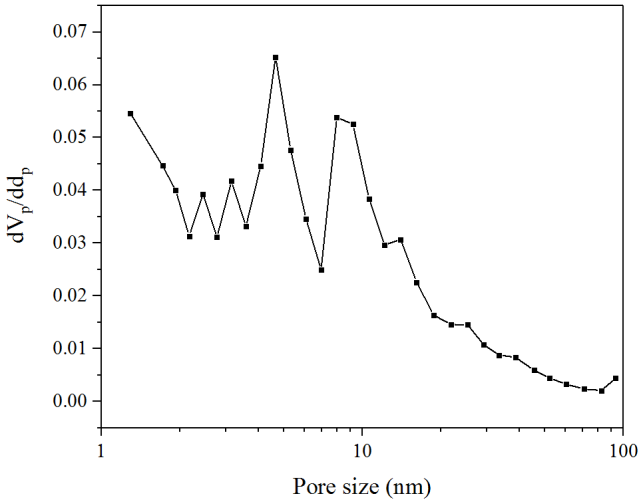

Figure 4. Pore size distribution obtained for the Ni-Mo/NG catalyst.

Specific surface area, total pore volume and mean pore size of the synthesized Ni-Mo/NG are given in Table 3 and compared with those of the industrial Ni-Mo/γ-Alumina catalyst.

Pore size distribution of the nanocatalyst is shown in Fig. 4, where it can be observed that peaks smaller than 10 nm are dominant in the synthesized Ni-Mo/NG. As can be observed in this figure, the pore size distribution is composed of two main peaks including 9-10 nm and the highest peak is 4 nm.

Table 3. BET surface area, pore volume and average pore diameter of the catalysts.

Characteristic/ Catalyst	BET Area (m^2/g)	Pore Volume (cm^3/g)	Pore Size (nm)
Industrial catalyst	216.53	0.548	6.51
Nanoporous Graphene	629.3	2.03	12.9
Ni-Mo/NG	228.58	1.0696	18.718

FE-SEM images of the Ni-Mo/NG catalyst are shown in Fig. 5, in which the sheets of nanoporous graphene can be observed. Also, an elemental map of the sample is shown in Fig. 5 from which uniform distribution of the metals over nanoporous graphene is clear. ICP results for the Ni-Mo/NG are shown in Table 4 and compared with those of the industrial catalyst. Two important parameters of the synthesized nanocatalyst, i.e. Ni/Mo weight ratio and total metal loading (wt.%) are close to those of the industrial catalyst so that the effect of nanoporous graphene as support can be compared with γ-Alumina.

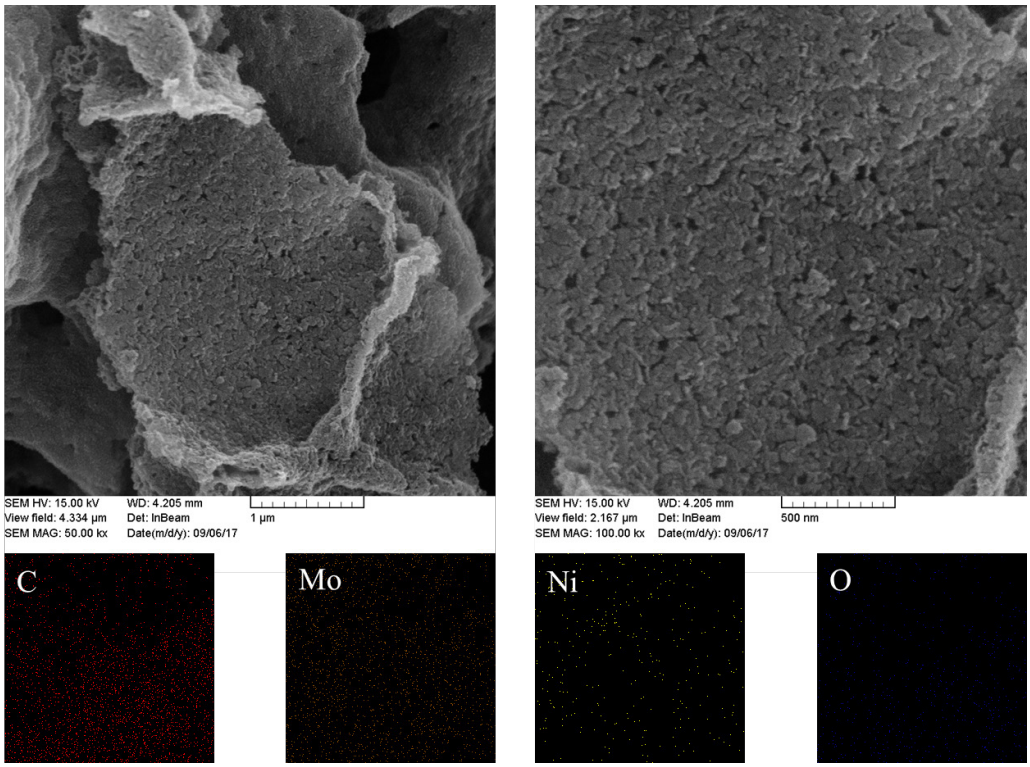

Figure 5. FE-SEM images of the Ni-Mo/NG catalyst (upper part) and elemental mapping of the sample (bottom part).

Table 4. Metal precursors in their oxide phase.

Characteristic / Catalyst	ICP Ni/Mo (wt. ratio)	ICP Total metal loading (wt. %)
Industrial catalyst	0.24	14.1
Ni-Mo/NG	0.25	13.5

XRD patterns of the nanoporous graphene support and the Ni-Mo/NG catalyst are shown in Fig. 6. The main peaks at 2θ of 26.4 and 43.6° are recognized for pure nanoporous graphene which are characteristic peaks of the graphitic structure. In the XRD pattern of the Ni-Mo/NG sample, characteristic peaks of the nanoporous graphene support are formed; however, their intensities have decreased. In addition to characteristic peaks of the graphitic structure, peaks at 2θ of 23.43 and 25.8° are observed, which correspond to the MoO_3 crystalline phase JCPDS 00-005-0508). The nickel loaded on nanoporous graphene was less than 3.5 wt.%, so no clear peak was observed in the XRD pattern of the Ni-Mo/NG catalyst.

In the TPR curve of the Ni-Mo/NG sample (Fig. 7), one continuous peak was observed which started at 400°C and ended at 700°C. It has been reported (Bunch and Ozkan, 2002) that various molybdenum oxides and nickel oxides are reduced in the range of 400-500°C to form oxides with different oxidation states, i.e. reduction of Mo^{+6} to Mo^{+4} occurs in the temperature range of 400-500°C which is eventually converted to metallic Mo at higher temperatures

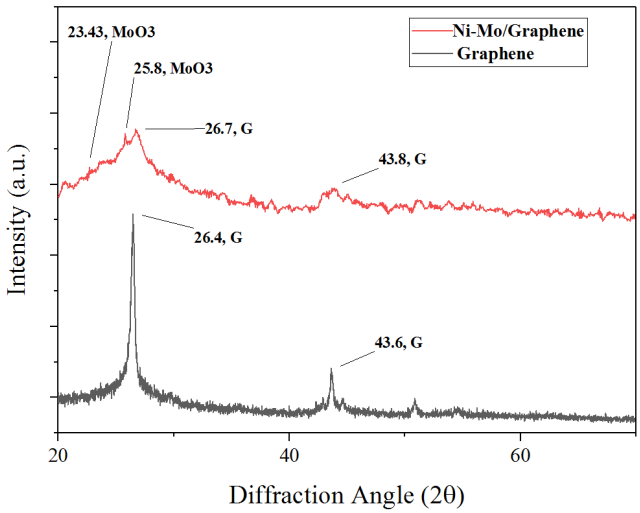

Figure 6. XRD pattern of nanoporous Graphene (gray color) and the Ni-Mo/NG catalyst (red color).

(Bunch and Ozkan, 2002; Purón et al., 2017; Wang et al., 2015).

Catalyst activity (evaluation of HDS and HDN reactions)

The catalytic activity of the novel synthesized Ni-Mo/NG catalyst was studied and compared with the Ni-Mo/γ-Alumina industrial catalyst. Specific gravity, RON, total sulfur (T.S.), R-SH compounds (mercaptans) and total nitrogen (T.N.) of the heavy naphtha feedstock are shown in Table 5. After

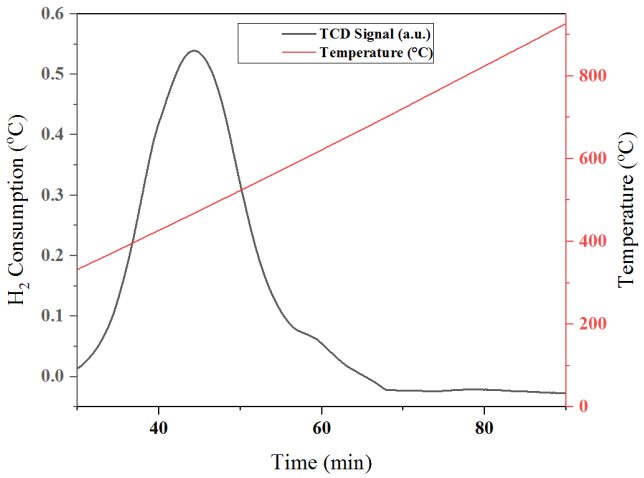

Figure 7. TPR of the synthesized Ni-Mo/NG catalyst.

Table 5. Physical properties of feedstock.

Sample/Analysis	Heavy naphtha	Test Method
Specific Gravity @15°C	0.7426	ASTM D4052
Total Sulfur, ppm	180	ASTM D5453
R-SH, ppm	18.9	ASTM D3227
Total Nitrogen, ppm	3.0	ASTM D4629
R.O.N	47	ASTM D2699

performing the reactions according to the mentioned operating conditions in Table 2, the product was carefully investigated.

ASTM D-86 of heavy naphtha in the feedstock and products of both catalysts are shown in Fig. 8, in which there is no significant difference between the product of Ni-Mo/γ-Alumina and the Ni-Mo/NG catalyst. Also, PIONA of the feedstock and products of each catalyst (after 24 h) are shown in Fig. 9. In this figure, it is observed that for naphthenes and paraffins, the reverse trend is obtained in which the Ni-Mo/NG catalyst has led to a lower amount of paraffins, whereas the lower amount of naphthenes was obtained with the industrial Ni-Mo/γ-Alumina catalyst.

For assessing the catalytic activity of the synthesized catalyst in HDS and HDN of heavy naphtha, the

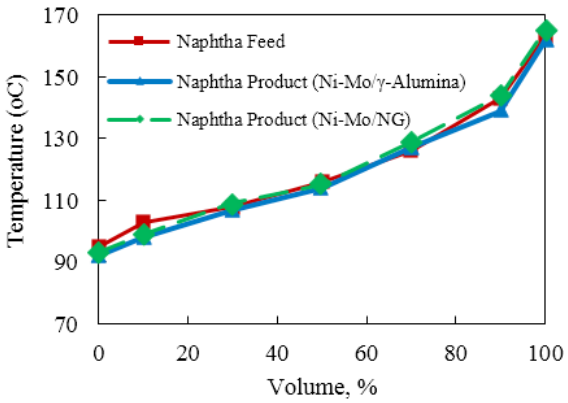

Figure 8. ASTM D-86 of heavy naphtha in feedstock and product of all catalysts.

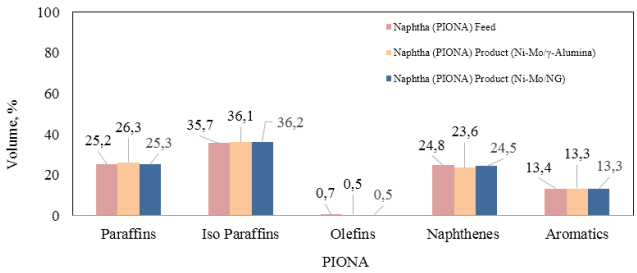

Figure 9. PIONA of heavy naphtha in feedstock and product of all catalysts.

following equation was used for calculating the catalytic conversion of sulfur and nitrogen compounds in heavy naphtha:

$$Xi = \left(\frac{ci_0 - ci}{ci_0} \right) \times 100 \quad (1)$$

In this equation, Xi corresponds to conversion (%) of total sulfur (T.S.), R-SH compounds (mercaptans) and total nitrogen (T.N.). Ci_0 shows the T.S., R-SH, and T.N. in the initial heavy naphtha before catalytic reactions (ppm by wt.) and Ci is related to these compounds in the treated naphtha (ppm by wt.).

Conversion of sulfur and nitrogen compounds by the novel Ni-Mo/NG catalyst is shown in Fig. 10 and compared with the catalytic activity of the Ni-Mo/γ-Alumina industrial catalyst. It is observed that, by adopting the Ni-Mo/NG catalyst, HDS and HDN activity has been increased compared with the industrial catalyst. By loading the Ni-Mo oxides over nanoporous graphene, after 240 h the total sulfur conversion was increased by 2.7% compared with the industrial catalyst. The Ni-Mo/NG catalyst performed better regarding the total nitrogen conversion, for which 99.4% T.N. conversion was obtained after 24 h. Also, with respect to the catalytic conversion of R-SH compounds, the catalytic activity of the Ni-Mo/NG catalyst was considerably enhanced compared with the industrial catalyst.

It can be observed that the synthesized Ni-Mo/NG catalyst has shown higher activity for T.S., T.N., and R-SH conversion: 99.5, 99.4 and 99.3% after 24 h and also 98.1, 97.5 and 98.7% after 240 h, respectively. This implies that this novel nanocatalyst has acceptable performance in long periods. By using nanoporous graphene as NiMo catalyst support rather than γ-Alumina, conversions of T.S., T.N., and R-SH were increased by 1.4, 1.5 and 0.8% after 24 h and by 2.7, 1.8 and 1.5% after 240 h, respectively. Considering the obtained results, it can be deduced that the synthesized Ni-Mo/NG catalyst has admissible selectivity toward removal of the main components in the heavy naphtha feedstock such as mercaptans (R-SH), sulfides (R_2S), disulfides (RSSR), thiophene (T)

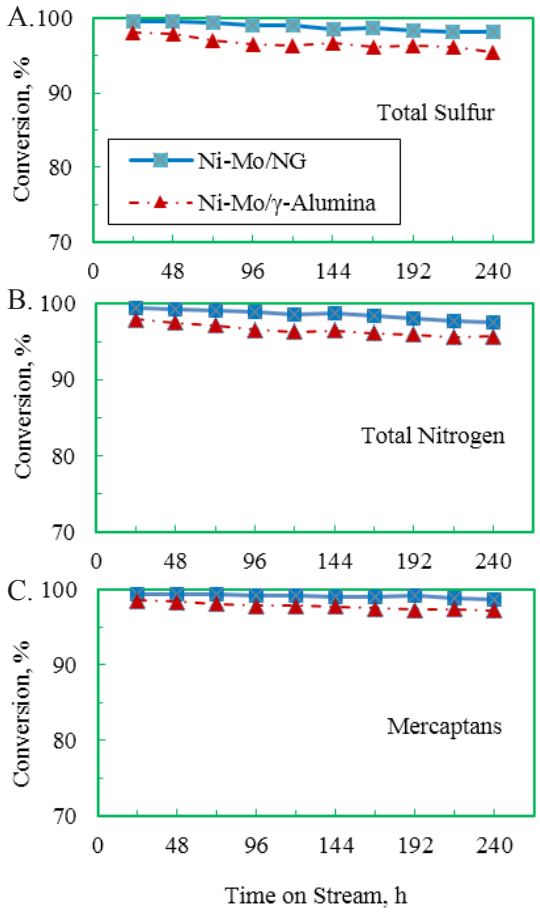

Figure 10. Conversion (%) of T.S., R-SH and T.N. of heavy naphtha over different catalysts. Reaction conditions: T=290°C, P=30 bar, LHSV=3.3 h^{-1} and H_2/HC=100 NL/L.

and its alkylated derivatives, benzothiophene (BT) and alkylated benzothiophenes (Song, 2003).

After a long period of using the catalysts, they are deactivated by coke formation and sintering of the catalysts. In these situations, to compensate the activity of catalysts in industrial reactors, the inlet reactor temperature is increased, which leads to an increment of the reactor bed temperature. By increasing the activity of the catalyst, the selectivity will be increased; however, the lighter compounds in the feedstock would be cracked to undesirable by-products. In this condition, some portion of the liquid phase will be converted to a gaseous phase, which leads to a gradual decrement of the liquid product yield. The amount of liquid product loss strongly depends on the catalyst life cycle and the severity of the reaction conditions, which are determined by the amount of the inlet reactor temperature increment (Ancheyta et al., 2003; Clark et al., 2001; Dufresne, 2007). In this study, the inlet reactor temperature was constant for 240 h on stream. Fig. 11 shows the amount of liquid product recovery during this period. Minor impact on the reduction of liquid product recovery was observed

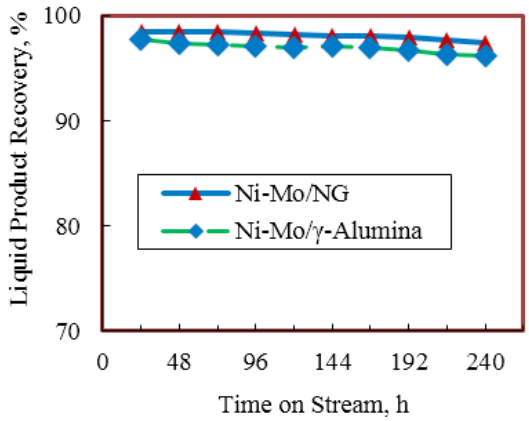

Figure 11. Lquid products recovery (%) for the different catalysts.

because the inlet temperature of the reactor was constant. As the Ni-Mo/NG catalyst was more active than Ni-Mo/γ-Alumina, its slope was much smoother than the alumina supported catalyst during the TOS. The overall decrease in the amount of liquid product recovery for the Ni-Mo/NG and the Ni-Mo/γ-Alumina catalyst was obtained as 1.1% and 1.6%, respectively.

The higher catalytic activity of the novel Ni-Mo/NG catalyst in comparison to the industrial Ni-Mo/γ-Alumina catalyst can be attributed to positive effects of the nanoporous graphene support. As specific surface area and total pore volume of the nanoporous graphene are higher than those of the γ-Alumina support, the active sites are distributed more preferentially. Better distribution and exposure of the active sites lead to higher contact with sulfur and nitrogen compounds, which results in enhanced catalytic activity. Thus, it is concluded that using nanoporous graphene as support for loading metal oxides can considerably enhance the HDS and HDN performance of the conventional catalysts.

CONCLUSION

In this research, a novel Ni-Mo loaded Nanoporous Graphene catalyst (Ni-Mo/NG) was synthesized by incipient wetness impregnation. The catalytic activity of the synthesized nanocatalyst was studied in HDS and HDN of the heavy naphtha. XRD patterns showed that the MoO_3 crystalline phase had been successfully loaded on nanoporous graphene and total metal loading (wt.%) was determined by the ICP method as 13.5 wt.% (Ni/Mo (wt. ratio)= 0.25), which is close to that of the industrial Ni-Mo/γ-Alumina catalyst. Performance of the catalyst regarding the conversion of total sulfur, total nitrogen and R-SH compounds was assessed at 290°C and 30bar. HDS and HDN activity of the Ni-Mo/NG catalyst were considerably higher than the industrial catalyst in which total sulfur, total nitrogen, and R-SH compound conversions of 99.5,

99.4 and 99.3% were obtained for our novel Ni-Mo/ nanoporous graphene catalyst.

REFERENCES

Al-Daous, M. A., Graphene–MoS_2 composite: Hydrothermal synthesis and catalytic property in hydrodesulfurization of dibenzothiophene. Catalysis Communications, 72, 180-184 (2015). https://doi.org/10.1016/j.catcom.2015.09.030

Ancheyta, J., Betancourt, G., Centeno, G., and Marroquín, G., Catalyst deactivation during hydroprocessing of Maya heavy crude oil.(II) Effect of temperature during time-on-stream. Energy & Fuels, 17(2), 462-467 (2003). https://doi.org/10.1021/ef0201883

Bunch, A. Y., and Ozkan, U. S., Investigation of the reaction network of benzofuran hydrodeoxygenation over sulfided and reduced Ni–Mo/Al_2O_3 catalysts. Journal of catalysis, 206(2), 177-187 (2002). https://doi.org/10.1006/jcat.2001.3490

Clark, P., Li, W., and Oyama, S. T., Synthesis and activity of a new catalyst for hydroprocessing: tungsten phosphide. Journal of catalysis, 200(1), 140-147 (2001). https://doi.org/10.1006/jcat.2001.3189

Dong, K., Ma, X., Zhang, H., and Lin, G., Novel MWCNT-Support for Co-Mo Sulfide Catalyst in HDS of Thiophene and HDN of Pyrrole. Journal of Natural Gas Chemistry, 15(1), 28-37 (2006). https://doi.org/10.1016/S1003-9953(06)60004-2

Dufresne, P., Hydroprocessing catalysts regeneration and recycling. Applied Catalysis A: General, 322, 67-75 (2007). https://doi.org/10.1016/j.apcata.2007.01.013

Eswaramoorthi, I., Sundaramurthy, V., Das, N., Dalai, A. K., and Adjaye, J., Application of multi-walled carbon nanotubes as efficient support to NiMo hydrotreating catalyst. Applied Catalysis A: General, 339(2), 187-195 (2008). https://doi.org/10.1016/j.apcata.2008.01.021

Fan, D.-H., Niu, D.-J., and Huang, K.-J., Simultaneous determination of adenine and guanine in DNA based on carboxylic acid functionalized graphene. Sensors and Actuators B: Chemical (2010). https://doi.org/10.1016/j.snb.2010.03.023

Gao, Q., Ofosu, T. N. K., Ma, S.-G., Komvokis, V. G., Williams, C. T., and Segawa, K., Catalyst development for ultra-deep hydrodesulfurization (HDS) of dibenzothiophenes. I: Effects of Ni promotion in molybdenum-based catalysts. Catalysis Today, 164(1), 538-543 (2011). https://doi.org/10.1016/j.cattod.2010.10.016

González-Cortés, S. L., Rodulfo-Baechler, S. M., Xiao, T., and Green, M. L., Rationalizing the catalytic performance of γ-alumina-supported Co (Ni)–Mo (W) HDS catalysts prepared by urea-matrix combustion synthesis. Catalysis letters, 111(1), 57-66 (2006). https://doi.org/10.1007/s10562-006-0130-y

Hajjar, Z., Kazemeini, M., Rashidi, A., and Bazmi, M., In Situ and Simultaneous Synthesis of a Novel Graphene-Based Catalyst for Deep Hydrodesulfurization of Naphtha. Catalysis letters, 145(9), 1660-1672 (2015). https://doi.org/10.1007/s10562-015-1563-y

Hajjar, Z., Kazemeini, M., Rashidi, A., and Bazmi, M. (2016). Graphene based catalysts for deep hydrodesulfurization of naphtha and diesel fuels: A physiochemical study. Fuel, 165, 468-476 (2016a). https://doi.org/10.1016/j.fuel.2015.10.040

Hajjar, Z., Kazemeini, M., Rashidi, A., and Soltanali, S., Optimizing parameters affecting synthesis of a novel Co–Mo/GO catalyst in a Naphtha HDS reaction utilizing D-optimal experimental design method. Journal of the Taiwan Institute of Chemical Engineers, 78, 566-575 (2017a). https://doi.org/10.1016/j.jtice.2017.06.048

Hajjar, Z., Kazemeini, M., Rashidi, A., Soltanali, S., and Bahadoran, F., Naphtha HDS over Co-Mo/Graphene catalyst synthesized through the spray pyrolysis technique. Journal of Analytical and Applied Pyrolysis, 123, 144-151 (2017b). https://doi.org/10.1016/j.jaap.2016.12.013

Hajjar, Z., Kazemeini, M., Rashidi, A., and Tayyebi, S., Artificial intelligence techniques for modeling and optimization of the HDS process over a new graphene based catalyst. Phosphorus, Sulfur, and Silicon and the Related Elements, 191(9), 1256-1261 (2016b). https://doi.org/10.1080/10426507.2016.1166428

Huang, K.-J., Niu, D.-J., Sun, J.-Y., Han, C.-H., Wu, Z.-W., Li, Y.-L., and Xiong, X.-Q., Novel electrochemical sensor based on functionalized graphene for simultaneous determination of adenine and guanine in DNA. Colloids and Surfaces B: Biointerfaces, 82(2), 543-549 (2011). https://doi.org/10.1016/j.colsurfb.2010.10.014

Huirache-Acuña, R., Pawelec, B., Loricera, C. V., Rivera-Muñoz, E. M., Nava, R., Torres, B., and Fierro, J. L. G., Comparison of the morphology and HDS activity of ternary Ni(Co)-Mo-W catalysts supported on Al-HMS and Al-SBA-16 substrates. Applied Catalysis B: Environmental, 125, 473-485 (2012). https://doi.org/10.1016/j.apcatb.2012.05.034

Julkapli, N. M., and Bagheri, S., Graphene supported heterogeneous catalysts: An overview. International Journal of Hydrogen Energy, 40(2), 948-979 (2015). https://doi.org/10.1016/j.ijhydene.2014.10.129

Khorami, P., and Kalbasi, M., Hydrodesulphurisation activity of CoMo catalyst supported on multi wall carbon nanotube: sulphur species study. Journal of Experimental Nanoscience, 6(4), 349-361 (2011). https://doi.org/10.1080/17458080.2010.497948

Klimov, O. V., Nadeina, K. A., Dik, P. P., Koryakina, G. I., Pereyma, V. Y., Kazakov, M. O., and Noskov, A. S., CoNiMo/Al_2O_3 catalysts for deep hydrotreatment of vacuum gasoil. Catalysis Today, 271, 56-63 (2016). https://doi.org/10.1016/j.cattod.2015.11.004

Liu, H., Li, Y., Yin, C., Wu, Y., Chai, Y., Dong, D., and Liu, C., One-pot synthesis of ordered mesoporous NiMo-Al_2O_3 catalysts for dibenzothiophene hydrodesulfurization. Applied Catalysis B: Environmental, 198, 493-507 (2016). https://doi.org/10.1016/j.apcatb.2016.06.004

Liu, N., Wang, X., Xu, W., Hu, H., Liang, J., and Qiu, J., Microwave-assisted synthesis of MoS_2/graphene nanocomposites for efficient hydrodesulfurization. Fuel, 119, 163-169 (2014). https://doi.org/10.1016/j.fuel.2013.11.045

Mendoza-Nieto, J. A., Robles-Méndez, F., and Klimova, T. E., Support effect on the catalytic performance of trimetallic NiMoW catalysts prepared with citric acid in HDS of dibenzothiophenes. Catalysis Today, 250, 47-59 (2015). https://doi.org/10.1016/j.cattod.2014.05.002

Miller, J., Reagan, W., Kaduk, J., Marshall, C., and Kropf, A., Selective hydrodesulfurization of FCC naphtha with supported MoS_2 catalysts: the role of cobalt. Journal of catalysis, 193(1), 123-131. https://doi.org/10.1006/jcat.2000.2873

Purón, H., Pinilla, J. L., Montoya de la Fuente, J., and Millán, M., Effect of metal loading in NiMo/Al2O3 catalysts on Maya vacuum residue hydrocracking. Energy & Fuels, 31(5), 4843-4850 (2017). https://doi.org/10.1021/acs.energyfuels.7b00104

Rambabu, N., Badoga, S., Soni, K. K., Dalai, A. K., and Adjaye, J., Hydrotreating of light gas oil using a NiMo catalyst supported on activated carbon produced from fluid petroleum coke. Frontiers of Chemical Science and Engineering, 8(2), 161-170 (2014). https://doi.org/10.1007/s11705-014-1430-1

Shan, S., Yuan, P., Han, W., Shi, G., and Bao, X., Supported NiW catalysts with tunable size and morphology of active phases for highly selective hydrodesulfurization of fluid catalytic cracking naphtha. Journal of catalysis, 330, 288-301 (2015). https://doi.org/10.1016/j.jcat.2015.06.019

Soghrati, E., Kazemeini, M., Rashidi, A. M., and Jozani, K. J., Preparation and Characterization of Co-Mo Catalyst Supported on CNT Coated Cordierite Monoliths Utilized for Naphta HDS Process. Procedia Engineering, 42, 1484-1492 (2012). https://doi.org/10.1016/j.proeng.2012.07.541

Song, C., An overview of new approaches to deep desulfurization for ultra-clean gasoline, diesel fuel and jet fuel. Catalysis Today, 86(1), 211-263 (2003). https://doi.org/10.1016/S0920-5861(03)00412-7

Sundaramurthy, V., Dalai, A., and Adjaye, J., HDN and HDS of different gas oils derived from Athabasca bitumen over phosphorus-doped NiMo/γ-Al_2O_3 carbides. Applied Catalysis B: Environmental, 68(1-2), 38-48 (2006). https://doi.org/10.1016/j.apcatb.2006.07.014

Vonortas, A., and Papayannakos, N., Kinetic Study of the Hydrodesulfurization of a Heavy Gasoil in the Presence of Free Fatty Acids Using a CoMo/γ-Al_2O_3 Catalyst. Industrial & Engineering Chemistry Research, 53(23), 9646-9652 (2014). https://doi.org/10.1021/ie5006492

Wang, H., Xiao, B., Cheng, X., Wang, C., Zhao, L., Zhu, Y., and Lu, X., NiMo catalysts supported on graphene-modified mesoporous TiO_2 toward highly efficient hydrodesulfurization of dibenzothiophene. Applied Catalysis A: General, 502, 157-165 (2015). https://doi.org/10.1016/j.apcata.2015.05.028

Yu, Z., Fareid, L. E., Moljord, K., Blekkan, E. A., Walmsley, J. C., and Chen, D., Hydrodesulfurization of thiophene on carbon nanofiber supported Co/Ni/Mo catalysts. Applied Catalysis B: Environmental, 84(3), 482-489 (2008). https://doi.org/10.1016/j.apcatb.2008.05.013

Zepeda, T. A., Pawelec, B., Obeso-Estrella, R., Díaz de León, J. N., Fuentes, S., Alonso-Núñez, G., and Fierro, J. L. G., Competitive HDS and HDN reactions over NiMoS/HMS-Al catalysts: Diminishing of the inhibition of HDS reaction by support modification with P. Applied Catalysis B: Environmental, 180, 569-579 (2016). https://doi.org/10.1016/j.apcatb.2015.07.013